LITHOS 450-451 (2023) 107205

Contents lists available at ScienceDirect

LITHOS

journal homepage: www.elsevier.com/locate/lithos

The mechanism responsible for the geochemical diversity of the Putuoshan volcanic-plutonic complex and its implications for the late Mesozoic crustal evolution of the Cathaysia Block, Southeast China

Jiao-Long Zhao [a,*], Liang Liu [b,*], Hang Xu [c], Er-Teng Wang [a]

[a] School of Earth Sciences, Key Laboratory of Mineral Resources in Western China (Gansu Province), Lanzhou University, Lanzhou 730000, China
[b] State Key Laboratory of Ore Deposit Geochemistry, Institute of Geochemistry, Chinese Academy of Sciences, Guiyang 550081, China
[c] State Key Laboratory for Mineral Deposits Research, School of Earth Sciences and Engineering, Nanjing University, Nanjing 210023, China

ARTICLE INFO

Keywords:
Volcanic-plutonic complex
Crystal-melt segregation
Mush rejuvenation
Southeast China

ABSTRACT

Essential mechanisms for the geochemical diversity observed in a silicic igneous rock association, which is of paramount importance for understanding the differentiation and growth of continental crust, remain highly controversial. Here the issues are explored by comparing the Late Cretaceous intrusions (minor-phase miarolitic alkali-feldspar granite and main-phase alkali-feldspar granite) and coeval volcanic rocks (rhyolite and rhyodacite) within the Putuoshan (PTS) volcanic-plutonic complex in the coastal area of southeast (SE) China. Zircon U—Pb ages indicate that the rhyolite, rhyodacite, minor-phase granite and the previously studied main-phase granite are nearly contemporaneous (ca. 98–94 Ma), but the coexisting dacites are obviously earlier at ca. 160 Ma. The dacites show adakitic geochemical characteristics and extremely enriched Nd—Hf isotopic compositions with Paleoproterozoic model ages, suggesting their derivation from remelting of Paleoproterozoic basement rocks in a thickened lower crust. In contrast, the coexisting Late Cretaceous volcanic and intrusive rocks have comparable and relatively depleted Nd—Hf isotopic compositions. Our data, combined with previous studies suggest that parental magmas of these Late Cretaceous magmatic rocks were derived from partial melting of juvenile crust with varying degrees of involvement of mantle-derived melts, and the observed compositional variation are mainly controlled by crystal-melt segregation and rejuvenation of crystal mush facilitated by recharge of hot mafic magmas in the shallow magma reservoir. The Jurassic and Late Cretaceous magmatic rocks within the PTS complex were generated in an advancing subduction compressive regime and a retreating subduction extensional regime of the paleo-Pacific plate, respectively. The gradually increasing tectonic extension during the Cretaceous due to slab rollback and the induced underplating of depleted mantle-derived magmas not only gave rise to the continental rejuvenation of SE China but also are the main driving mechanism of this Late Cretaceous long-lived transcrustal magma system.

1. Introduction

The processes giving rise to silicic magma are fundamental to the differentiation and growth of continental crust and also closely related to the mineralization of rare earth elements (REE) and rare metals (Lee and Morton, 2015; Lundstrom and Glazner, 2016; Wu et al., 2020). Although extensive research has been done, the origin of silicic magma remains highly controversial (Curry et al., 2021; Frost and Frost, 2011). Some scholars proposed that parental magma of the silicic magma is produced by partial melting of various source materials ranging from crustal assemblages to oceanic slab, even metasomatized mantle wedge, and then retains a high proportion of melt with few crystals in magma chambers. Subsequently, continuous fractional crystallization combined with or without assimilation gives rise to the formation of silicic magmatic rocks (Foley et al., 2002; Frost and Frost, 2011; Macpherson et al., 2006). On the contrary, a consensus has been emerging that melt-rich magma chambers are short-lived (Bachmann and Bergantz, 2004; Deering et al., 2016), and increasing studies proposed that silicic magmas are dominantly derived from extensive, long-lived "mushy" reservoirs through slow extraction of interstitial melts trapped within mush zones (Bachmann and Bergantz, 2004; Deering et al., 2016; Walker et al., 2007). Accordingly, questions arise as to how the almost

* Corresponding authors.
E-mail addresses: jlz@lzu.edu.cn (J.-L. Zhao), liuliang@vip.gyig.ac.cn (L. Liu), wanget19@lzu.edu.cn (E.-T. Wang).

https://doi.org/10.1016/j.lithos.2023.107205
Received 11 April 2023; Received in revised form 2 May 2023; Accepted 2 May 2023
Available online 5 May 2023

contemporaneous erupted silicic volcanic rocks and intruded plutonic rocks relate to each other in a single magmatic system, and what controls the compositional diversity observed in the volcanic-plutonic complex and composite granite pluton. The importance and potential impacts of understanding the origin of silicic magmatic rocks thus is not just a matter of discerning how Earth's continental crust formed, but also of predicting polymetallic mineralization (Bachmann et al., 2007; Lundstrom and Glazner, 2016).

The late Mesozoic geology of southeastern (SE) China is characterized by voluminous granite and their volcanic equivalents, as well as rare andesitic and mafic rocks (Fig. 1), which are commonly considered to be products of the subduction of the paleo-Pacific plate beneath SE China (Li and Li, 2007; Liu et al., 2020; Zhou et al., 2006). The Jurassic igneous rocks are mainly concentrated in the interior of SE China, whereas the Cretaceous ones mainly occur in the coastal region (Fig. 1). Moreover, recent studies recognize that there exist sporadically exposed Early-Middle Jurassic magmatic rocks within the coastal areas of SE China (Yuan et al., 2018; Zhao et al., 2021). The Cretaceous volcanic rocks in the coastal area of SE China erupted in multiple eruptive stages between 145 and 86 Ma and most of them are tightly temporal and spatial association with shallow intrusions in some calderas, constituting a voluminous volcanic–plutonic complex belt along the coastal area of SE China, such as Xiaoxiong and Daiyunshan complexes (Fig. 1, Li et al., 2022; Xu et al., 2021; Yan et al., 2016, 2018). In particular, some of them are closely associated with Be—Mo mineralization, such as the Zhangji, Xiapu, and Minhou complexes in coastal Zhejiang and Fujian Provinces (Fig. 1, Rao et al., 2022). Previous studies of the Cretaceous silicic magmatism in the coastal area mainly focused on intrusive rocks and various mechanisms have been proposed to explain their formation and relatively depleted Nd—Hf isotopic characteristics, including

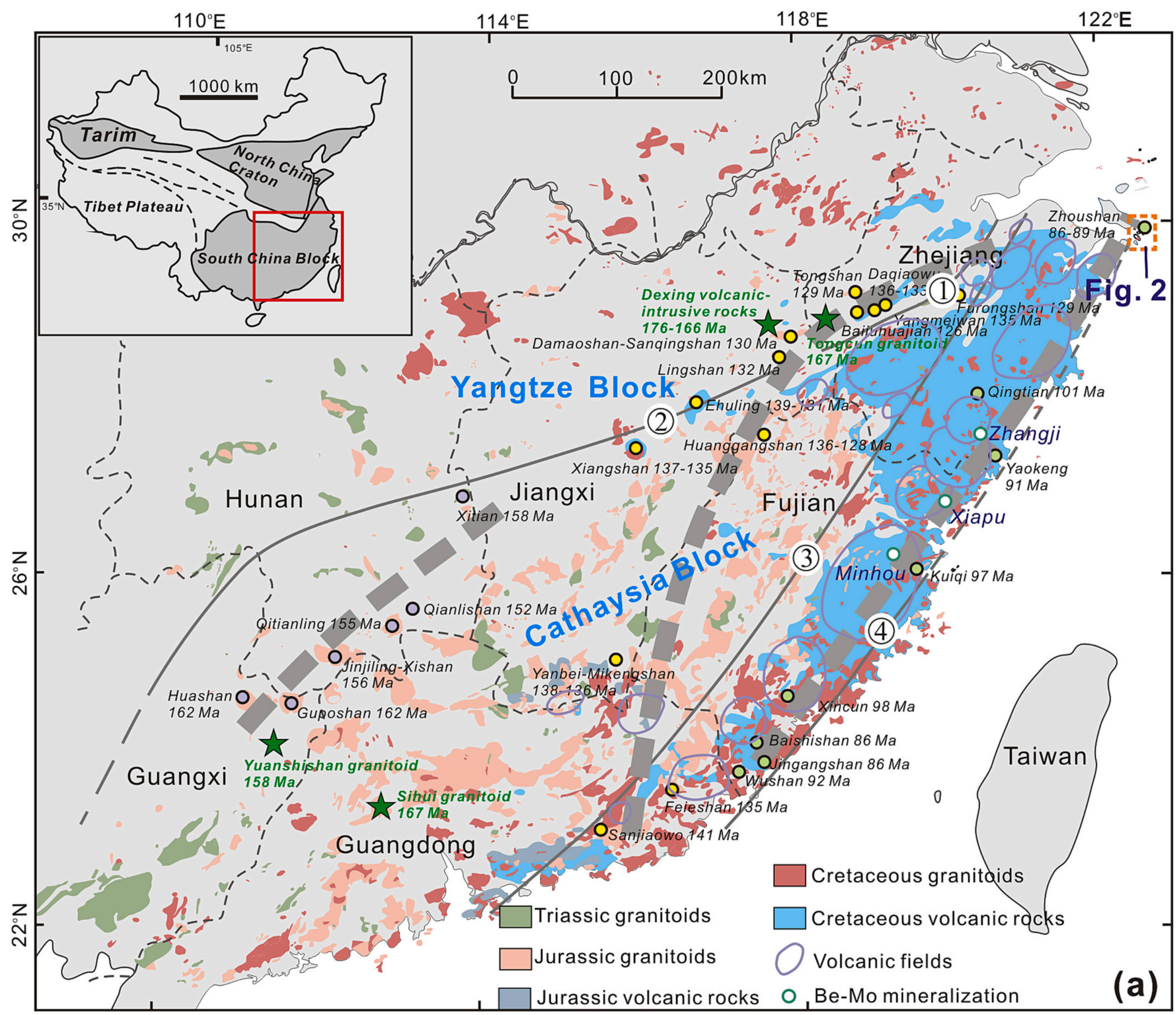

Fig. 1. (a) The distribution of Late Mesozoic igneous rocks in SE China and the location of the studied area (modified from Zhou et al., 2006, Rao et al., 2022, Xu et al., 2021). The pentagrams with green fill color represent Jurassic adakitic rocks in SE China. The circles with purple fill color represent Late Jurassic A-type granite, and the ones with yellow and light green fill colors represent Early Cretaceous A-type rocks, and Late Cretaceous A-type rocks, respectively. The dotted ashen lines delineate the Late Jurassic A-type rock belt, Early Cretaceous A-type rock belt and the Late Cretaceous A-type granite belts. Names of the fault zones: ① Jiangshan–Shaoxing fault; ② Pingxiang–Yushan fault; ③ Zhenghe–Dapu & Lishui-Yuyao fault; ④ Changle–Nan'ao fault. The cited geochronological data are from Peng et al. (2021), Qiu et al. (2013), Zhao et al. (2015, 2016), Zhou et al. (2012), Zhou et al. (2015), Zhong et al. (2013). (For interpretation of the references to color in this figure legend, the reader is referred to the web version of this article.)

mixing of crustal- and mantle-derived magmas, melting of juvenile crust, or a combination of both (Li et al., 2015; Liu et al., 2013, 2018; Zhao et al., 2015, 2016). Moreover, the timing of the juvenile crust formation is also controversial, ranging from Precambrian to late Mesozoic time (Gan et al., 2022; Jiang et al., 2015; Xu et al., 2007). Interestingly, the existing researches show that the Cretaceous silicic magmas in the coastal region range from metaluminous to strongly peraluminous and from calc-alkaline to peralkaline in compositions, and could be divided into I-type and A-type subtypes (Chen et al., 2019; Qiu et al., 2004; Wu et al., 2022; Xu et al., 2022; Yan et al., 2018; Yang et al., 2018), but essential mechanisms for their geochemical and lithological diversity within a suite need to be further clarified.

The Putuoshan (PTS) volcanic-plutonic complex in northeastern Zhejiang Provinces, SE China, mainly consists of I-type alkali-feldspar granite and peralkaline A-type granite with subordinate miarolitic alkali-feldspar granite and volcanic rocks (Fig. 2, Qiu et al., 2004; Zhao et al., 2016). More importantly, in addition to extensive Late Cretaceous magmatic rocks, our fieldwork newly discovered small-volume Middle-

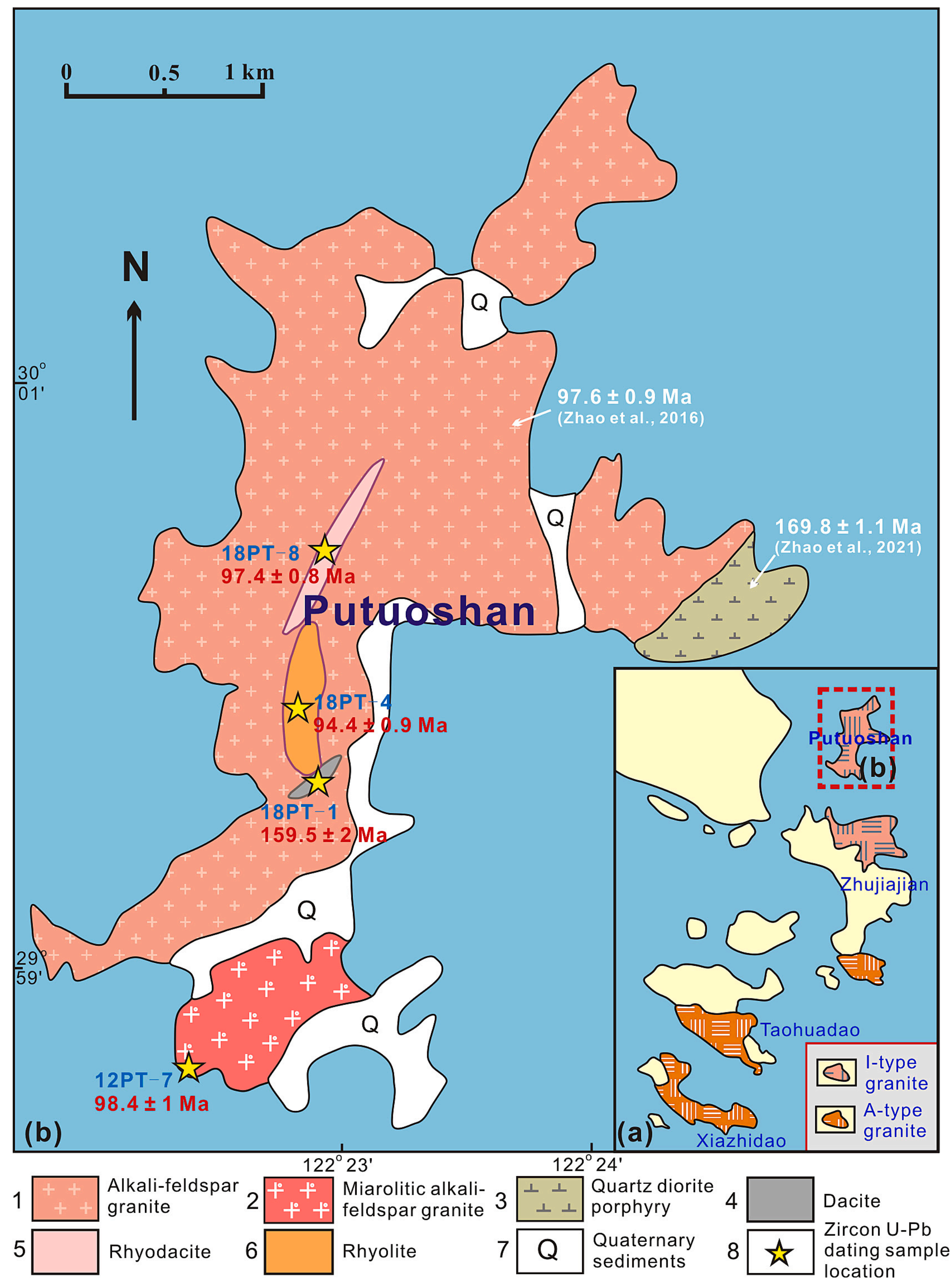

Fig. 2. (a) Simplified geological map of the Zhoushan archipelago, showing the location of Putuoshan Island. (b) Simplified geological map of the Putuoshan (PTS) volcanic-plutonic complex (modified after Zhang et al., 2005).

Late Jurassic volcanic-subvolcanic rocks derived from remelting of ancient crustal materials within the complex, which could place important constraints on the nature of the regional crystalline basement that generally remains unclear (Zhao et al., 2021 and this study). The PTS complex thus provides an excellent target to study the evolution and modification of continental crust and the linkage of these Late Cretaceous coexisting volcanic and plutonic rocks. Unfortunately, previous studies mainly focused on Late Cretaceous main-phase granite and peralkaline A-type granite, and paid less attention to the coeval volcanic rocks and minor-phase miarolitic granite because of minimal exposure, and the key factors for controlling chemical compositions of the various Late Cretaceous rock types within the PTS volcanic-plutonic complex are still not clear (Qiu et al., 2004; Zhang et al., 2005; Zhao et al., 2016, 2021).

In this study, comprehensive petrographical, geochronological and geochemical analyses were conducted for the volcanic rocks and minor-phase miarolitic alkali-feldspar granite from the PTS volcanic-plutonic complex. Our new data combined with previous studies aim to elucidate magma sources of the distinct rocks, especially the genetic relationship of the Late Cretaceous various rock types within the complex, place new constraints on the late Mesozoic crustal growth and geodynamic evolution of SE China, and offer insights into the fundamental magmatic processes of the Earth's crust.

2. Geological setting and sample description

The Cathaysia block, which is widely recognized that amalgamated with the Yangtze block along the Jiangshan–Shaoxing fault during early Neoproterozoic to form the South China block, is characterized by large volumes of late Mesozoic lavas and their intrusive counterparts (Fig. 1), with quite sparsely exposed Precambrian metamorphic basement (Xia et al., 2018; Yao et al., 2019). The late Mesozoic intrusive rocks are varied, comprising mainly high-K calc-alkaline I- and A-type granite and lesser amounts of syenite, quartz diorite, and gabbro (Liu et al., 2020; Zhou et al., 2006). These A-type granites are widely distributed in the Cathaysia block, and form three nearly parallel, NE-trending belts with Late Jurassic, Early Cretaceous and Late Cretaceous ages, respectively (Fig. 1), in addition to the ca. 200–170 Ma EW-striking belt in the Nanling region (He et al., 2010; Peng et al., 2021). Both the Late Jurassic and Early Cretaceous A-type granite belts are situated in the inland region, with ages of ca. 165–150 Ma and ca. 140–125 Ma (Chen et al., 2016; Jiang et al., 2015; Peng et al., 2021; Zhou et al., 2012; Zhou et al., 2015), respectively, whereas the Late Cretaceous A-type granite belt with ages from 101 to 86 Ma is developed in the coastal region (Fig. 1, Qiu et al., 2004; Zhao et al., 2015, 2016). Volcanic rocks are mainly erupted in the Cretaceous and generally crop out along the coastal area of SE China. They are generally grouped by the widespread unconformity into the lower and upper volcanic series and a volcanic hiatus at ca. 120–110 Ma had been identified between them (He and Xu, 2012).

The studied Putuoshan (PTS) volcanic-plutonic complex is a multi-staged volcanic-intrusive complex, predominantly made of granites with lesser amounts of dacitic-rhyolitic volcanic rocks and quartz diorite porphyry (Table 1). The ages of main-phase I-type alkali-feldspar granites and peralkaline A-type granites have been constrained by zircon U—Pb dating, and are in the range of 98–96 Ma and 89–86 Ma, respectively (Zhao et al., 2016). The quartz diorite porphyry exposed in the northeastern part of the PTS pluton is intruded by main-phase I-type alkali-feldspar granite, shows adakitic geochemical characteristics and is dated at ca. 170 Ma (Zhao et al., 2021). The minor-phase miarolitic alkali-feldspar granite within the southern part of the Putuoshan island (Fig. 2) is classified as an A-type aluminous subtype and has single zircon U—Pb age of 93 Ma (Qiu et al., 2004). They are subvolcanic, medium-grained (Fig. 3a), and consist of quartz (35–40 vol%), perthite (50–60 vol%), plagioclase (15–10 vol%), and minor biotite (<3 vol%) (Fig. 3b and c), with accessory spessartine, zircon, apatite and titanite. Miarolitic cavities are fairly common and are often filled by aggregates of pegmatitic quartz and alkali-feldspar (Fig. 3a) and sometimes, by aluminous-rich minerals, such as spessartine, muscovite and even corundum (Qiu et al., 2004). Microgranular mafic enclaves (MMEs) are rare within this lithological unit (Fig. 3a) but are widely scattered throughout the main-phase granite (Fig. 3m, Xie et al., 2004; Zhao et al., 2016).

Table 1
Summary of the volcanic and intrusive rocks within the PTS pluton in coastal Zhejiang Province.

Lithology	Zircon U—Pb age	SiO_2 (wt%)	A/CNK	$\varepsilon_{Nd}(t)$	Zircon $\varepsilon_{Hf}(t)$	Reference
Quartz diorite porphyry	169.8 ± 1 Ma	63.36 to 67.04	0.92 to 0.97	−18.1 to −17.7	-23.4 to −17.9	Zhao et al. (2021)
Dacite	159.5 ± 2 Ma	60.23 to 67.76	0.99 to 1.04	−12.2	-18.6 to −12.6	this study
Main-phase granite	97.6 ± 0.9 Ma	74.24 to 77.53	0.95 to 1.11	−7.1 to −7.0	-7.9 to −3.1	Zhao et al. (2016)
Minor-phase granite	98.4 ± 1 Ma	75.36 to 78.09	0.98 to 1.06	−7.4	-7.8 to −3.5	this study
Rhyodacite	97.4 ± 0.8 Ma	72.10 to 72.98	1.09 to 1.14	−6.3 to −6.2	-7.3 to −5.9	this study
Rhyolite	94.4 ± 0.9 Ma	74.74 to 77.18	1.04 to 1.15	−6.9 to −6.7	-7.0 to −4.3	this study

A/CNK: whole-rock molar $Al_2O_3/(CaO + Na_2O + K_2O)$ values.

The dacitic-rhyolitic volcanic rocks in this study, which are present in the upper part of the PTS granite intrusion, had been eroded, and are composed of dacite, rhyodacite, and rhyolite, as shown in Fig. 2. They exhibit porphyritic texture and massive (Fig. 3). The PTS dacites are in grey (Fig. 3d), and contain ~50 vol% phenocrysts of quartz, plagioclase and alkali-feldspar, and similar microcrystalline minerals in the groundmass (Fig. 3e and f). Quartz phenocrysts are generally rounded in shape, displaying resorption texture (Fig. 3e). The PTS rhyodacites are light grey (Fig. 3g), and contain ~35 vol% phenocrysts of alkali-feldspar, plagioclase and quartz, and ~ 65 vol% matrix of quartz, feldspar, and accessory zircon, and Fe—Ti oxides (Fig. 3h and i). The PTS rhyolites are off-white (Fig. 3j). The phenocrysts (~25 vol%), ranging in diameter from 1 to 4 mm, are dominated by quartz (~15 vol%), alkali-feldspar (~7 vol%) and plagioclase (~3 vol%). Subhedral quartz and plagioclase phenocrysts have resorbed cores and are commonly surrounded by alkali feldspar (Fig. 3k and l). The groundmass shows microcrystalline and micrographic textures (Fig. 3l), and is composed mainly of quartz and K-feldspar and a few opaque oxides. MMEs are rarely observed in these PTS volcanic rocks.

3. Geochronology

Zircon grains from the PTS volcanic–subvolcanic rocks are prismatic, euhedral, transparent, and colorless to pale yellow. They range from 80 to 200 μm in length, with length/width ratios of 1:1–3:1. In cathodoluminescence (CL) images (Fig. 4), all of the analyzed zircons exhibit oscillatory zoning or occasional typical zoning absorption, and most have relatively high Th/U ratios (0.54–4.85), indicating a magmatic origin (Corfu et al., 2003). The analytical results of zircon U—Pb dating are listed in Supplementary Table 1 and presented graphically in Fig. 4.

Nineteen analyses from dacite sample 18PT–1 are concordant and yield $^{206}Pb/^{238}U$ ages between 156.0 ± 2 Ma and 160.5 ± 1, with a weighted mean $^{206}Pb/^{238}U$ age of 159.5 ± 2 Ma [mean square weighted deviation (MSWD) = 0.28, 2σ; Fig. 4a], representing the formation age of the PTS dacite. Sixteen analyses from sample 18PT–8 (PTS rhyodacite) are all concordant or near-concordant, and yield a weighted mean

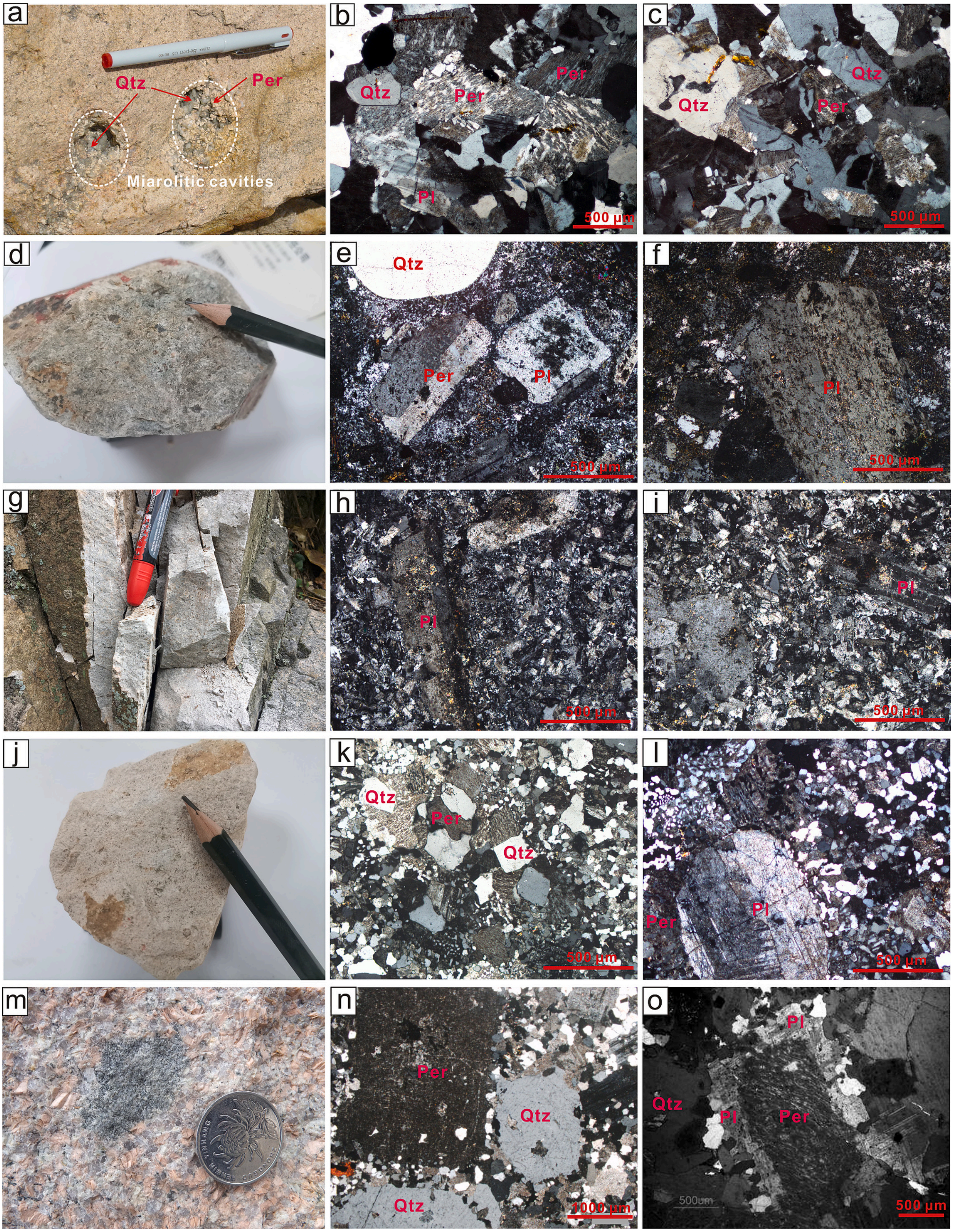

Fig. 3. Macroscopic photos and photomicrographs of the volcanic rocks and granites within the Putuoshan volcanic-plutonic complex. (a–c) PTS minor-phase miarolitic alkali-feldspar granite; (d–f) PTS dacite; (g–i) PTS rhyodacite; (j–l) PTS rhyolite; (m–o) PTS main-phase alkali-feldspar granite. Fig. 3o is from Zhang et al. (2005). All thin-section photos were taken under cross-polarized light. Mineral abbreviation: Per, perthite; Pl, plagioclase; Qtz, quartz.

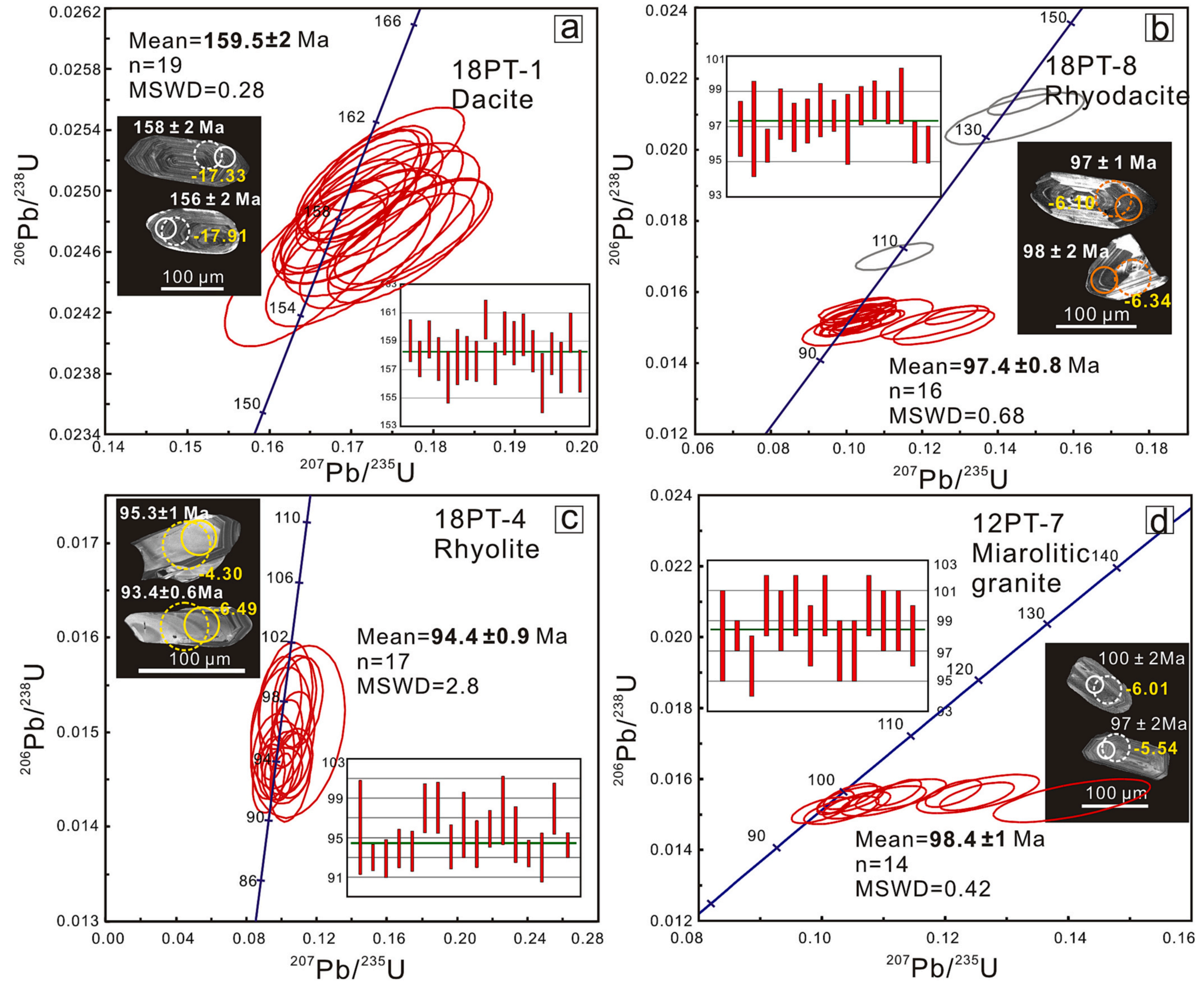

Fig. 4. Cathodoluminescence (CL) images of representative zircon grains and zircon U—Pb concordia diagrams for the PTS volcanic rocks and minor-phase miarolitic alkali-feldspar granite. (a) PTS dacite; (b) PTS rhyodacite; (c) PTS rhyolite; (d) PTS minor-phase miarolitic alkali-feldspar granite. Grey analyses (zircon grains spot no. 18PT8–01, 18PT8–14 and 18PT8–18) are not calculated for the $^{206}Pb/^{238}U$ weighted mean age of 18PT–8 sample.

$^{206}Pb/^{238}U$ age of 97.4 ± 0.8 Ma (MSWD = 0.68, 2σ; Fig. 4b), which is considered the crystallization age of the PTS rhyodacite. Three grains record older $^{206}Pb/^{238}U$ ages of 133.3 ± 3 Ma, 136.3 ± 2 Ma and 108.7 ± 2 Ma, which may represent captured grains. Seventeen analyses on zircon crystals from sample 18PT–4 (PTS rhyolite) yield $^{206}Pb/^{238}U$ ages between 98.0 ± 1.3 Ma and 92.9 ± 1.0 Ma, with a weighted mean of 94.4 ± 0.9 Ma (MSWD = 2.8, 2σ; Fig. 4c), representing the magma crystallization age of the PTS rhyolite. Fourteen zircons from the sample 12PT–7 (PTS minor-phase miarolitic granite) yield a weighted-mean $^{206}Pb/^{238}U$ age of 98.4 ± 1 Ma (MSWD = 0.42, 2σ; Fig. 4d), representing the magma crystallization age of the PTS minor-phase miarolitic granite.

4. Geochemistry and isotopic composition

4.1. Whole-rock major and trace elements

The results are listed in Supplementary Table 2. The volcanic rocks within the PTS volcanic-intrusive complex range from intermediate to felsic in composition, with SiO_2 contents of 60.23–67.76 wt% for the dacite, 72.10–72.98 wt% for the rhyodacite, and 74.74–77.18 wt% for the rhyolite (Fig. 5a). The minor-phase miarolitic alkali-feldspar granites are highly evolved with restricted SiO_2 contents of 75.36–78.09 wt% (Fig. 5a). All samples from the PTS volcanic-subvolcanic rocks are K_2O-enriched, have high contents of $Na_2O + K_2O$ varying from 6.95 to 8.78 wt%, and plot within the high-K calc-alkaline series on a SiO_2–K_2O diagram (Fig. 5a). The PTS dacite and miarolitic alkali-feldspar granite samples are metaluminous to weakly peraluminous with A/CNK values (molar ratio $Al_2O_3/(CaO + Na_2O + K_2O)$) from 0.99 to 1.04 and 0.98 to 1.06, respectively, while the PTS rhyolite and rhyodacite samples are peraluminous with A/CNK ratio values of 1.04–1.15 and 1.09–1.14, respectively (Fig. 5b).

Except for the PTS rhyolite, all samples from the PTS volcanic–subvolcanic rocks have high and variable concentrations of total rare earth elements (REE) varying from 87.3 ppm to 189 ppm. They are enriched in light REEs and large ion lithophile elements (LILE; e.g., Rb, Cs, and Pb), and depleted in high field strength elements (HFSE; e.g., Nb and Ta) (Fig. 6). In addition, the PTS dacites have lower Y and heavy REEs, and much higher Sr/Y and La/Yb ratios compared to the PTS Cretaceous volcanic-intrusive rocks, showing adakitic geochemical affinities (Figs. 5c and 6). Notably, the PTS rhyolites are characterized by pronounced enrichments in Rb, Th, U, Pb and Nb, and depletions in Ba, Sr, P

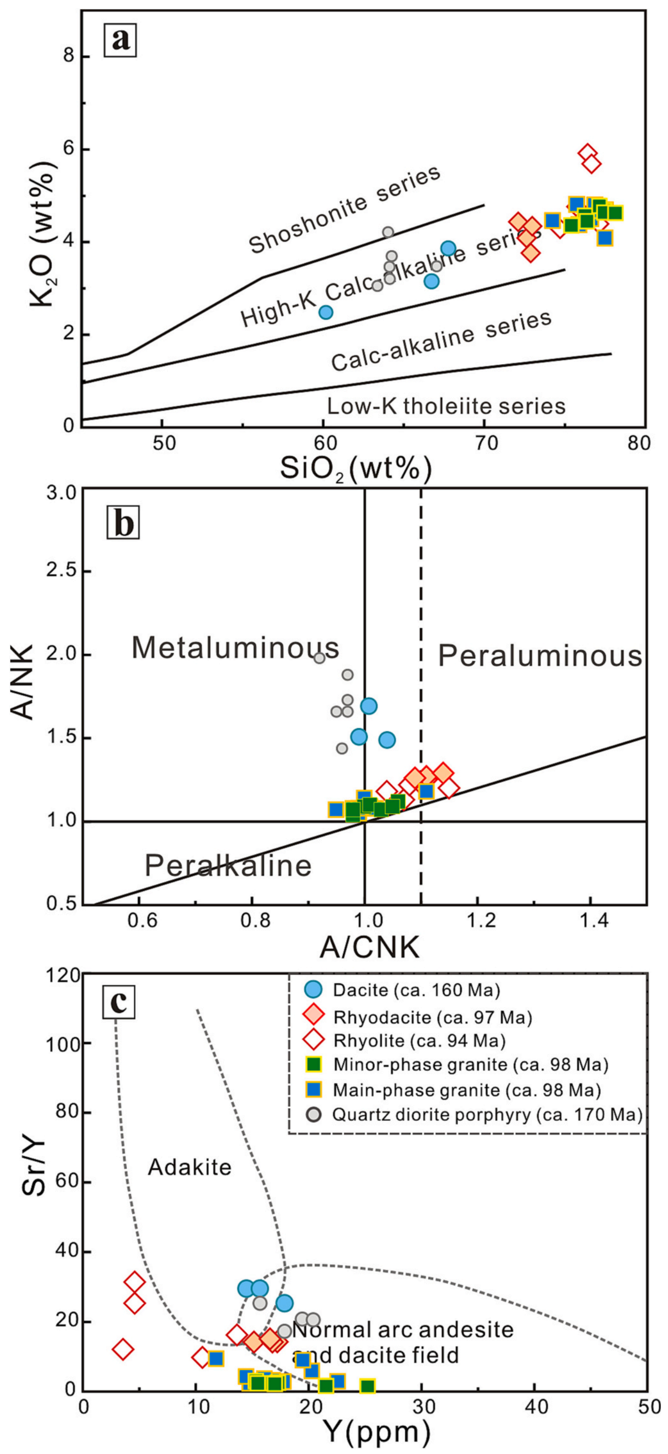

Fig. 5. Chemical classification of rocks from the Putuoshan volcanic-plutonic complex. (a) K_2O vs. SiO_2 diagram (Peccerillo and Taylor, 1976); (b) A/NK vs. A/CNK diagram (Maniar and Piccoli, 1989); (c) Sr/Y vs. Y diagram (Defant and Drummond, 1990).

and Ti, and show a continuous REE variation, which is characterized by a gradual depletion in REEs (Fig. 6). Furthermore, chondrite-normalized REE patterns for the PTS rhyolites show typical REE tetrad effect with $TE_{1,3}$ (quantification factor of tetrad effect) of 0.96–1.23.

4.2. Whole-rock Sr—Nd isotopes

Measured whole-rock Sr—Nd isotopic data for the PTS volcanic–sub-volcanic rocks are listed in Supplemental Table 2 and plotted in Fig. 7a. The Late Jurassic dacite exhibits an initial $^{87}Sr/^{86}Sr$ ratio of 0.7123 and $\varepsilon_{Nd}(t)$ values of −12.2 with two-stage Nd isotopic model ages of 1.94 Ga. In contrast, the Late Cretaceous samples from the PTS complex in this study give relatively homogeneous and more depleted Sr—Nd isotopic compositions, with initial $^{87}Sr/^{86}Sr$ ratios of 0.7124 to 0.7081 and $\varepsilon_{Nd}(t)$ values of −7.4 to −6.2, and their two-stage Nd model ages vary from 1.51 to 1.40 Ga, similar to those of the main-phase granite (Fig. 7).

4.3. Zircon Lu—Hf isotopes

In-situ Lu—Hf isotopic analyses of zircons from the PTS volcanic–sub-volcanic rocks are listed in Supplemental Table 3 and plotted in Fig. 8. Zircon grains from the PTS dacite (18PT-1) yield $\varepsilon_{Hf}(t)$ values varying from −18.6 to −12.6, and the corresponding two-stage Hf model ages (T_{DM2}) vary from 2.01 to 2.39 Ga. Zircon grains from the PTS rhyodacite (18PT-8) yield $\varepsilon_{Hf}(t)$ values from −7.3 to −5.9, with T_{DM2} ages ranging from 1.54 to 1.63 Ga. Zircon grains from the PTS rhyolite (18PT-4) possess $\varepsilon_{Hf}(t)$ values ranging from −7.0 to −4.3, and the corresponding T_{DM2} varies from 1.60 to 1.43 Ga. Zircon grains from the PTS miarolitic granite (12PT-7) yield $\varepsilon_{Hf}(t)$ values ranging from −7.8 to −3.5, with T_{DM2} ages of 1.66–1.39 Ga. One inherited grain shows a more evolved $\varepsilon_{Hf}(t)$ value of −14.7 with T_{DM2} age of 2.12 Ga.

5. Discussion

5.1. Petrogenesis of the PTS volcanic-plutonic complex

The studied late Mesozoic PTS volcanic-plutonic rocks in northeastern Zhejiang Provinces are generated without coeval massive mafic rocks in this region, precluding their origin by extensive crystal fractionation from coeval mafic magmas. Moreover, they are metaluminous to peraluminous, and have relatively high SiO_2 and K_2O concentrations and low MgO (Mg# mostly <45), Cr, and Ni contents, supporting their crustal origin (Jiang and Zhu, 2017). However, the Late Jurassic dacites in the PTS complex have different whole-rock Sr—Nd and zircon Hf isotopic compositions from the coexisting Cretaceous magmatic rocks (Figs. 7 and 8), further revealing different sources or different petrogenetic processes.

The Late Jurassic PTS dacites show extremely enriched whole-rock Sr—Nd and zircon Hf isotope compositions with Paleoproterozoic model ages (2.01–2.39 Ga), reflecting their derivation predominantly from partial melting of the ancient continental crust. Moreover, in an $\varepsilon_{Nd}(t)$ versus age diagram (Fig. 7a), the PTS dacite falls within the field of the crustal basement of the Cathaysia block. It is suggested that the PTS dacites were derived solely from the partial melting of basement Paleoproterozoic crustal rocks of the Cathaysia block. In contrast, the studied Late Cretaceous magmatic rocks have higher whole-rock $\varepsilon_{Nd}(t)$ (−7.4 to −6.2) and $\varepsilon_{Hf}(t)$ (−7.8 to −3.5) values with younger T_{DM2} ages (1.50–1.40 Ga) than the coexisting PTS dacite and crustal basement of the Cathaysia block, and plot above the isotope evolution field for the basement rocks (Figs. 7 and 8), suggesting significant involvement of mantle materials in their origin, either directly by magma mixing or by remelting of juvenile mantle-derived materials (Qiu et al., 2012; Wong et al., 2009).

Existing petrographic, mineralogical and geochemical studies for the PTS main-phase granite and Cretaceous granitoids and related melanocratic microgranular enclaves in eastern Zhejiang Province clearly revealed that mixing between magmas derived from mantle and crustal rocks did have played a role in their generation (Liu et al., 2013; Xie et al., 2004; Yan and He, 2022; Zhang et al., 2005). However, major oxide and trace element signatures (e.g., low MgO, Cr and high SiO_2 contents) of the PTS main-phase granite and the studied PTS Late Cretaceous magmatic rocks could not be perfectly explained by the magma mixing model although their Sr—Nd isotopic feature can be well matched by the mixing of asthenosphere-derived melts with 45–55%

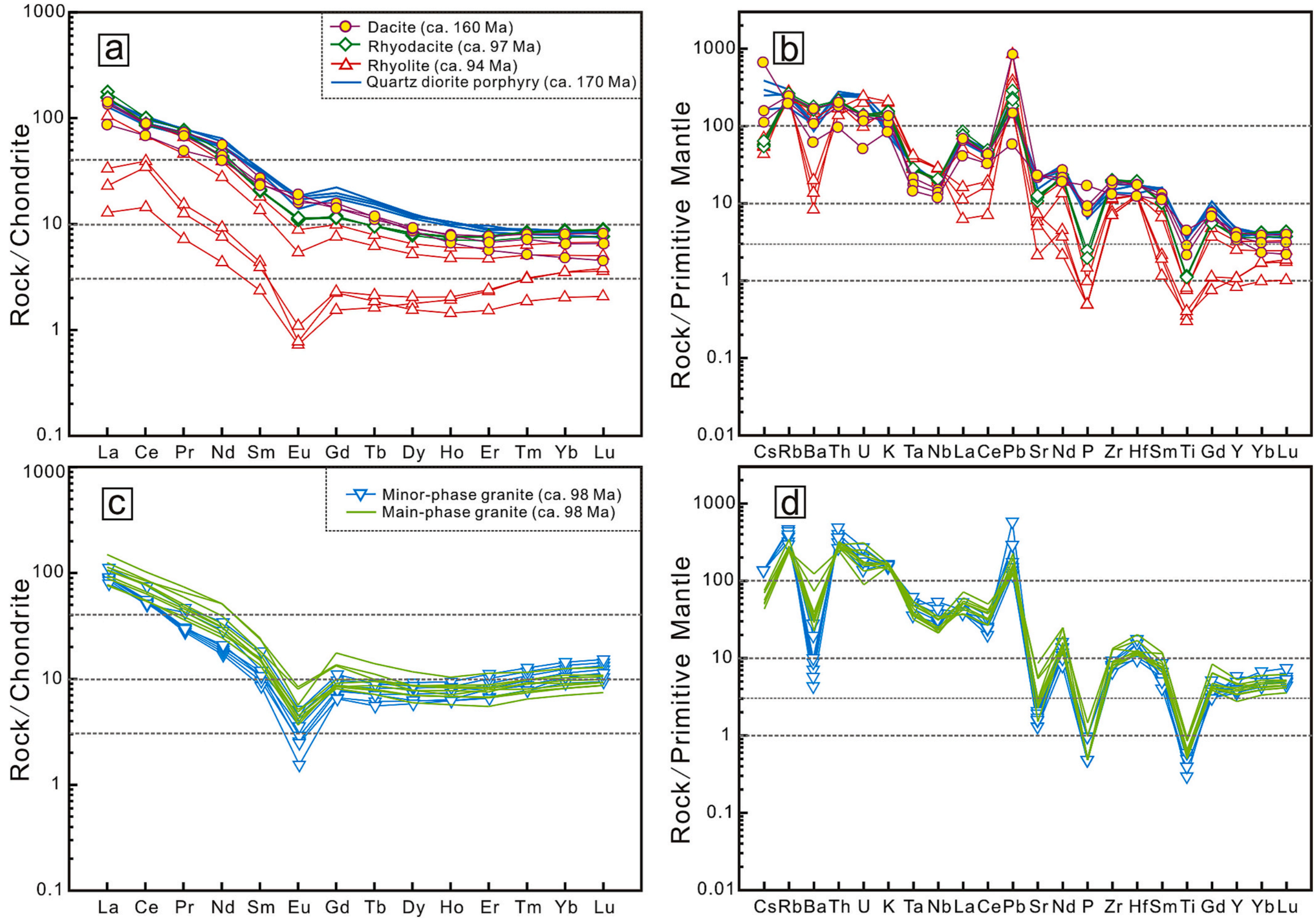

Fig. 6. Chondrite-normalized REE patterns (a and c) and primitive mantle (PM)-normalized trace element (b and d) diagrams for the Putuoshan volcanic-plutonic complex. Chondrite values are from Boynton (1984), and primitive mantle values are from McDonough and Sun (1995).

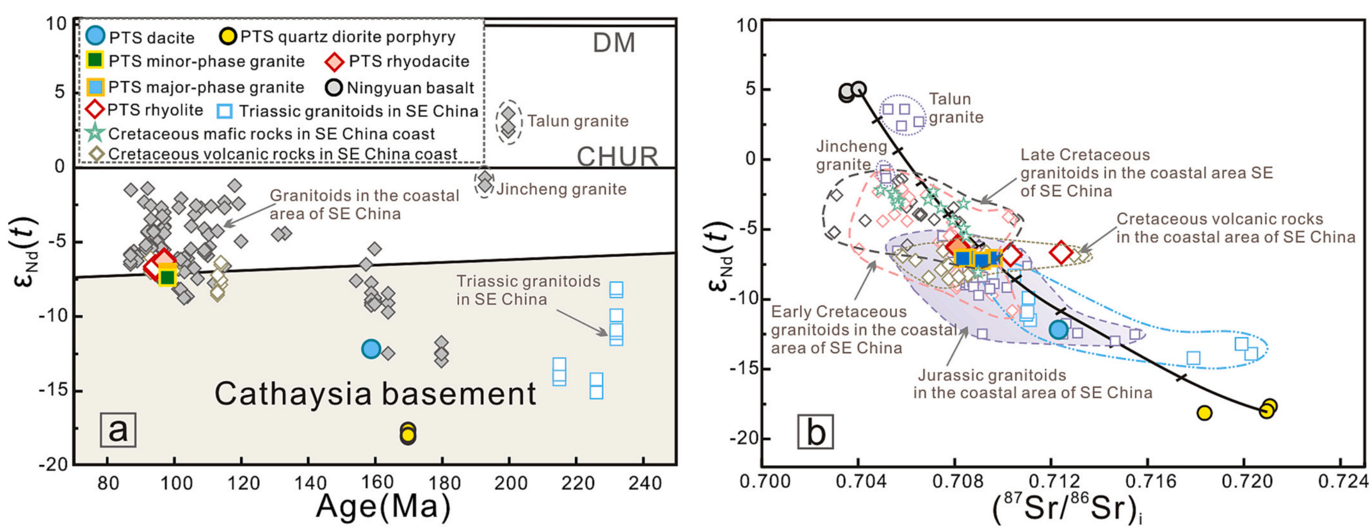

Fig. 7. (a) Whole-rock $\varepsilon_{Nd}(t)$ vs. age values of the Mesozoic granitoids and their equivalents from SE China. The area of the Cathaysia basement is modified from Chen and Jahn (1998). (b) Whole-rock $\varepsilon_{Nd}(t)$ vs. $(^{87}Sr/^{86}Sr)_i$ diagram for the Putuoshan volcanic-plutonic complex. The black line is a calculated binary mixing curve between possible mafic and felsic magma end-members. The depleted mantle is represented by the Ningyuan basalt in Hunan Province (Li et al., 2004). The crustal end-member is represented by the Putuoshan quartz diorite porphyry (Zhao et al., 2021). Tick marks represent 10% mixing increments. The data for the Mesozoic granitoids and their equivalents are from Liu et al. (2018, 2022), Chen et al. (2021), and Zhao et al. (2021) and references therein. The data for the Cretaceous mafic rocks are from Dong et al. (2008, 2010) and Li et al. (2014).

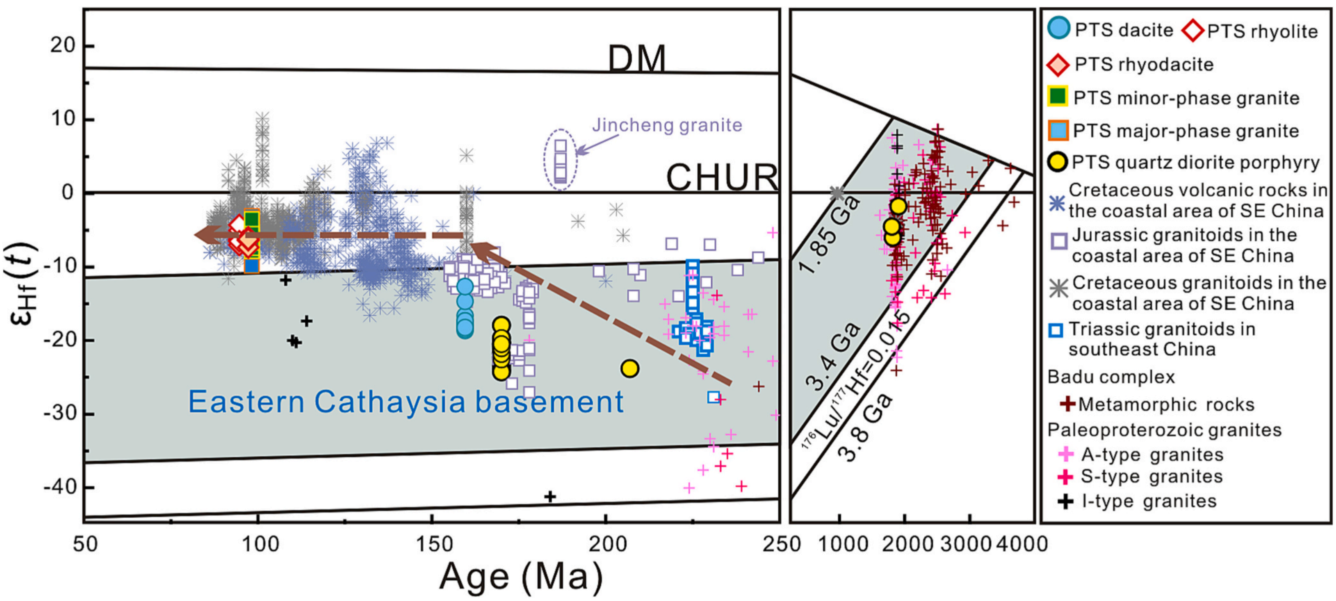

Fig. 8. Hf-isotope compositions of representative zircons from the Putuoshan volcanic-plutonic complex. The area of Eastern Cathaysia basement is after Xu et al. (2007). The data for the Badu complexes, and Paleoproterozoic A-type, I-type and S-type granites are the same as in Zhao et al. (2021). Data sources for Mesozoic granitoids and their equivalents in southeast China as in Fig. 7.

crust-derived melts (Fig. 7b). Moreover, the studied PTS Late Cretaceous highly evolved volcanic rocks and minor-phase miarolitic granite have relatively restricted variations in Sr—Nd isotopic composition, and both are roughly similar to those of the Cretaceous basalts and basic dykes from SE China (Fig. 7b, Dong et al., 2008, 2010; Li et al., 2014). Significantly, Cretaceous felsic magmatic rocks in the coastal region of SE China display comparable Nd—Hf isotopic compositions, which are more depleted than those of the Triassic and Jurassic magmatic rocks (Figs. 7 and 8). These provide first-order constraints on the petrogenesis of the studied Cretaceous magmatic rocks, namely that they are derived from a common source or its derivatives, and partial melting of juvenile crust exerts a crucial role in their generation. Therefore, it is suggested that their relatively depleted Sr-Nd-Hf isotopic characteristics are predominantly inherited from crustal magma sources with subordinate involvement of mantle-derived melt via magma mixing.

Collectively, the Late Jurassic PTS dacites were derived by partial melting of ancient basement rock in the Cathaysia block, while the studied PTS Late Cretaceous volcanic-plutonic rocks may be generated by partial melting of juvenile crust with variable involvement of mantle-derived melt.

5.2. Genetic relationship of the various Late Cretaceous rock types within the PTS complex

The studied PTS Late Cretaceous rhyolite, rhyodacite and minor-phase granite as well as the main-phase granite and peralkaline A-type granite spatially occur together (Fig. 2), constituting a typical volcanic–subvolcanic–intrusion association. Meanwhile, they have nearly indistinguishable zircon U—Pb ages, similar Sr—Nd and zircon Hf isotopic compositions and mineral assemblages, apart from the PTS peralkaline A-type granite that contains Na-rich mafic minerals (e.g., arfvedsonite and aegirine) and is considered to be the product of partial melting of the residual granulitic source after extraction of granitic melts (Jiang et al., 2022; Zhao et al., 2016). These characteristics not only support their derivation from a common magma source but also suggest a close genetic relationship among them. However, among the studied Late Cretaceous high-silica volcanic and intrusive rocks, the PTS rhyodacites are least evolved with strongly peraluminous geochemical characteristics and others are metaluminous to slightly peraluminous in composition (Fig. 5b). The mechanism responsible for the compositional diversity of these Late Cretaceous rocks remains poorly constrained.

The PTS miarolitic granites are more evolved than the main-phase granite, yielding compositional arrays that are consistent with fractional crystallization, as shown by their more significant depletions in Eu, Ba, Sr, P and Ti concentrations, and lower Zr content and Zr/Hf and CaO/Al_2O_3 ratios (Figs. 6 and 9). This suggests that fractional crystallization of plagioclase, alkali feldspar and minor zircon occurred and stayed as a residual phase in the shallow magma chamber during the generation of the PTS miarolitic granites. Especially, the PTS minor-phase miarolitic granites also show more elevated Nb, Ta, Y, Yb, and Lu contents than the main-phase granite (Fig. 6), indicating delayed crystallization of HFSE- and HREE-bearing accessory minerals in the high-silica magma in which the PTS minor-phase miarolitic granite crystallized. The main-phase granite and the minor-phase miarolitic granite are likely complementary components of fractional crystallization (Fig. 10). Namely, compatible elements (e.g., Sr, Ba, Zr, and Eu) are enriched in early crystallized minerals (in the main-phase granite), whereas incompatible elements (e.g., Rb and Th) are enriched in the residual melt (from which the minor-phase miarolitic granite crystallized). Therefore, we suggest that the former represents the cumulate residue while the latter largely (or entirely) represents the melt extracted from an upper crustal crystal mush, coinciding with the crystal mush model (Bachmann and Bergantz, 2004; Deering et al., 2011).

This inference is further supported by petrographic observations. Both types of granite within the PTS complex have identical mineral assemblage. There are abundant euhedral plagioclases in the PTS main-phase granite, and some of them are interconnected to form crystal aggregates, and are often encircled by interstitial alkali feldspar and quartz minerals (see Fig. 3b from Zhao et al., 2016), which represents frozen trapped pore melt (Holness, 2018). Moreover, coarse-grained, euhedral to subhedral alkali feldspar and quartz grains occur with interstitial residual felsic minerals (Fig. 3m and n). All of these observations indicate that plagioclase and early-stage alkali feldspar and quartz tend to construct the crystal framework of the main-phase alkali-feldspar granite, displaying a cumulate character (Vernon and Collins, 2011; Walker et al., 2007). These cumulate minerals are completely identical to those inferred from the above geochemical characteristics. In contrast, the PTS minor-phase miarolitic granites have

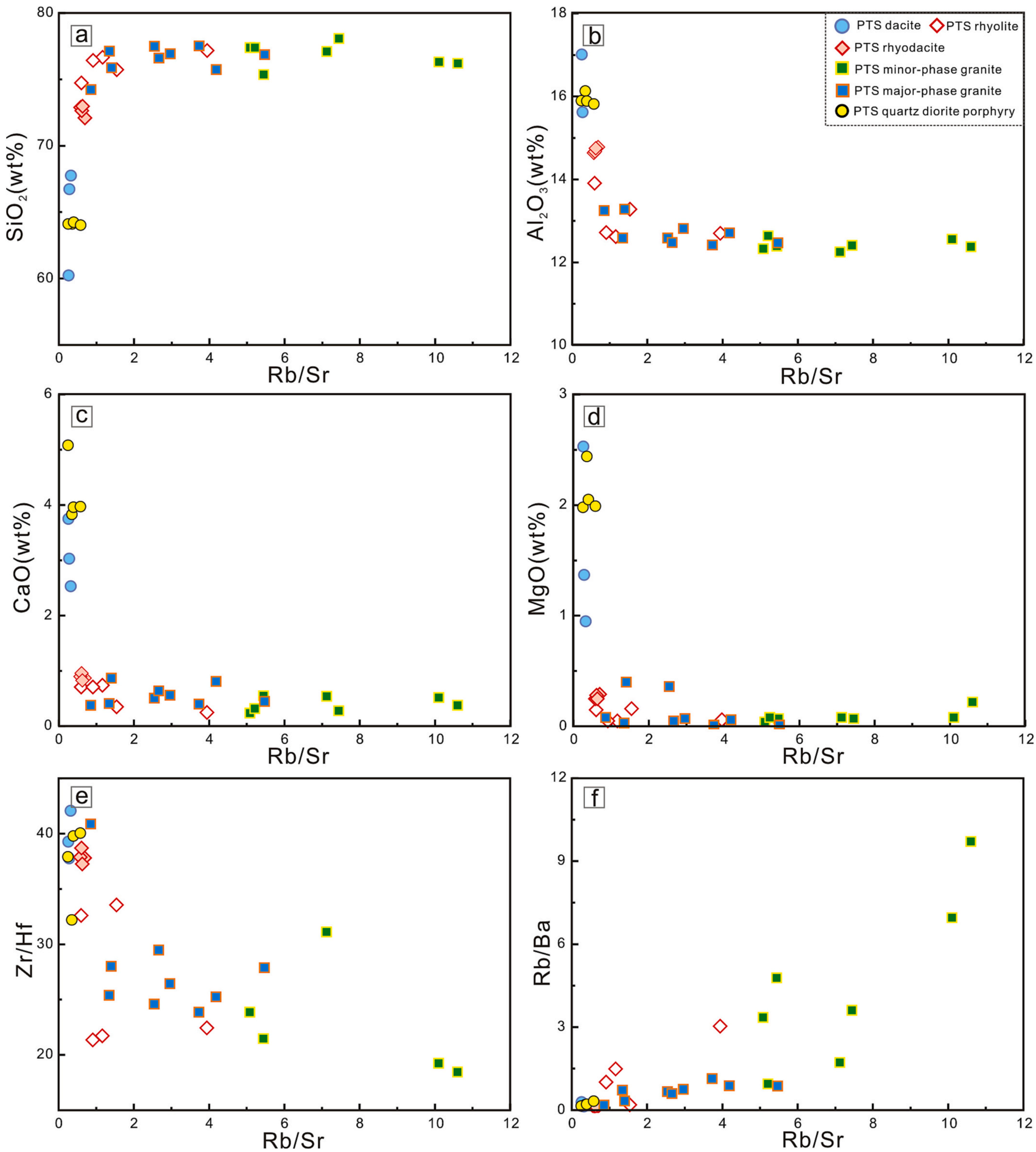

Fig. 9. Diagrams show the selected element or elemental ratio versus Rb/Sr for the Putuoshan volcanic-plutonic complex. (a) SiO_2, (b) Al_2O_3, (c) CaO, (d) MgO, (e) Zr/Hf, and (f) Rb/Ba.

petrographically less plagioclase, but more alkali feldspar (Fig. 3). Their mineral assemblages are dominated by simultaneously crystallized alkali feldspar and quartz, supporting that they crystallize from the extracted melt from a crystal mush at the top of the system. Therefore, a crystal mush model is invoked to explain the genetic relationship between the PTS minor-phase miarolitic granite and main-phase granite.

Compared with both the intrusive main- and minor-phase granites, the PTS erupted rhyodacites and two less evolved rhyolite samples (18PT–4 and 18PT–6) are strongly peraluminous in composition and have higher $Fe_2O_3^T$, MgO, Al_2O_3 and CaO contents and slightly negative Eu, Sr and Ba anomalies (Fig. 9), as well as somewhat more radiogenic Nd and Hf isotope compositions, which probably result from a shift in composition by addition of a hotter mafic recharge and explicitly assert the re-mobilization and/or partial melting of the pre-existed crystal

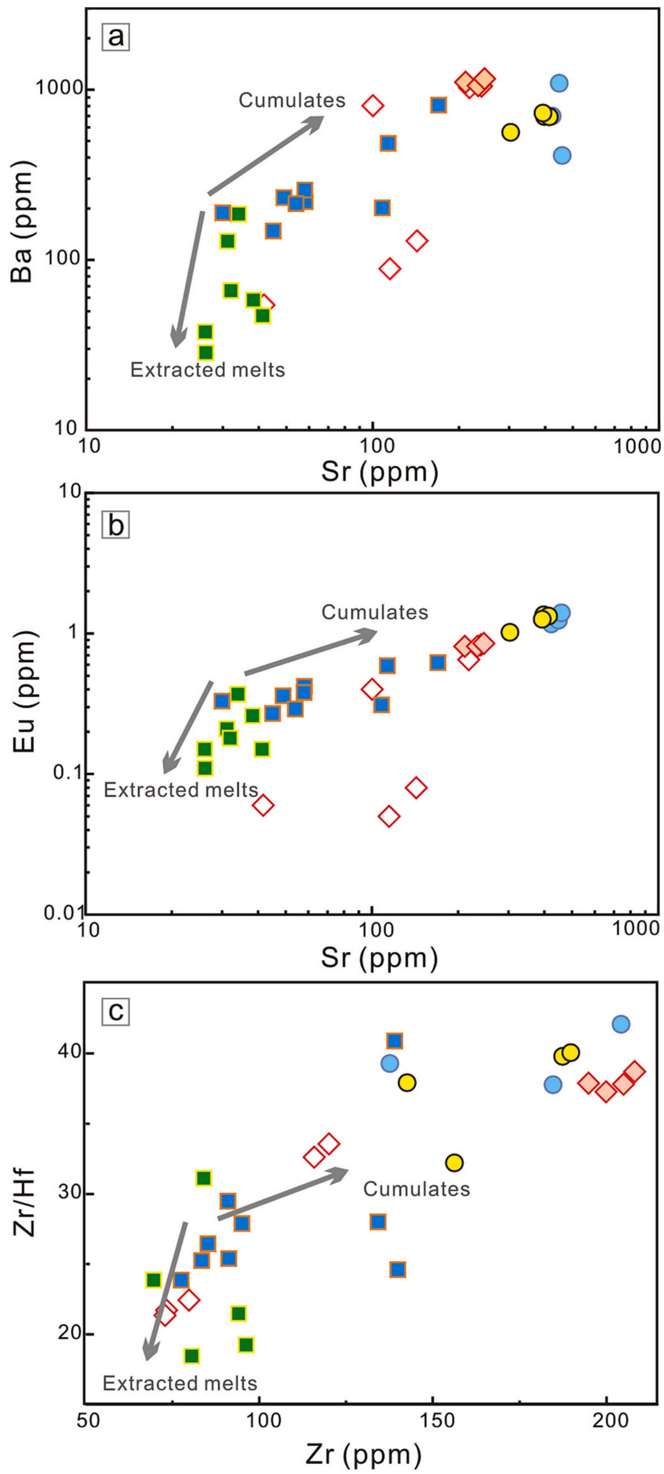

Fig. 10. Co-variations of element concentrations and elemental ratios of the Putuoshan volcanic-plutonic complex. (a) Ba vs. Sr; (b) Eu vs. Sr; (c) Zr/Hf vs. Zr. Symbols are the same as in Fig. 9.

mush (Du et al., 2022). This is further endorsed by three lines of petrographic and mineralogical evidences: (1) MMEs with the presence of euhedral acicular apatite and euhedral plagioclase showing reverse compositional zoning are scattered throughout the PTS main-phase alkali-feldspar granite (Xie et al., 2004); (2) Some ovoid alkali feldspar grains within the main-phase granite are mantled by plagioclase (Fig. 3o, Zhang et al., 2005), indicating a rapakivi texture, which is commonly associated with the rejuvenation of near-solidus crystal mush (Yin et al., 2021); (3) The quartz and feldspar crystals of the PTS erupted rhyodacites and rhyolite are typically resorbed and embayed, and some of the quartz grains are enclosed by alkali feldspar (Fig. 3k and l, Yan et al., 2022; Curry et al., 2021). That is, the addition of heat and/or volatile contents, both obtainable by recharge, triggered a limited remelting of a feldspar cumulate with minor small zircon crystal to produce a geochemically peraluminous, Zr-rich melt (Barnes et al., 2019; Curry et al., 2021; Yan et al., 2022), as these phases strongly partition Ba, Sr, Eu and Zr. The additions of these new liquids to the pre-existed interstitial melt subsequently form a new mixture of crystals and melt, from which the studied rhyodacites and rhyolites crystallized with the involvement of minor mafic recharge.

Petrographic observations suggest that the PTS rhyodacites show higher phenocryst contents than the coexisting rhyolites. Geochemically, the rhyodacites have less evolved geochemical compositions than those of the rhyolites (Figs. 6 and 9). These obviously reveal a vertical chemical and petrographical stratification in the magma chamber. Moreover, the rhyodacites appear to have more radiogenic Nd isotope compositions ($\varepsilon_{Nd}(t) = -6.3 \sim -6.2$) than the rhyolite ($\varepsilon_{Nd}(t) = -6.9 \sim -6.7$). It is therefore suggested that inadequate separation of mineral crystals from the newly formed viscous mixture of crystals and melt, would give rise to the variable extent of entrainment of suspended crystals in the melt from bottom to top, together with the contribution of mafic recharge magma, thus forming a relative crystal-poor cap (rhyolite) underlain by a crystal-rich zone (rhyodacite) with slightly more voluminous mantle-derived mafic magmas.

It should be noted that three samples from the PTS rhyolites show a spectacular tetrad effect in their REE distribution patterns. Zr and Hf are two geochemically very similar HFSEs and retain highly constant ratios in most terrestrial and extraterrestrial rocks (about 38 ± 2, Jahn et al., 2001). A highly fractionated Zr/Hf ratio (< 26) is a characteristic feature of aqueous systems rather than silicate systems (Bau, 1996; Irber, 1999). The PTS rhyolites with notable lanthanide tetrad effect show unusually low Zr/Hf ratios (22.4–21.4), strongly suggesting their origin is related to an aqueous system. Similarly, La/Nb and La/Ta ratios for these PTS rhyolite samples are lower than the common values of magmatic rocks, suggesting that the REE tetrad effect observed in the rhyolite was resulted from fluid–melt interactions at a late stage of magma evolution (Jahn et al., 2001). It is further supported by co-variations in Zr/Hf and $TE_{1,3}$ values from the rhyolite samples with no tetrad effect to highly evolved samples with the tetrad effect (Supplemental Table 2).

In summary, it is suggested that melts segregated from granitic crystal mush developed into the PTS minor-phase miarolitic granite, while the crystal-rich residues (mineral cumulates + interstitial residual melt) may be solidified to form the main-phase granites. Rejuvenation of the crystal mush due to repeated, hot, mafic magma replenishment resulted in the generation of strongly peraluminous felsic magma from which the PTS rhyodacite and the least evolved rhyolite crystallized. At the same time, the intense fluid-melt interaction resulted in the remarkable lanthanide tetrad effect of the three evolved samples from the PTS rhyolite.

5.3. *Geodynamic mechanism responsible for the generation of the late Mesozoic PTS volcanic-plutonic complex*

The newly discovered ca. 160 Ma dacites show adakite-like geochemical affinities, similar to those of the coexisting ca. 170 Ma quartz diorite porphyries, ca. 174 Ma granodiorites in the East China Sea Basin (Yuan et al., 2018; Zhao et al., 2021). It is suggested that these Middle-Late Jurassic magmatic rocks in the coastal area of SE China were formed by partial melting of the thickened lower continental crust with garnet and little or no plagioclase stable within the residual assemblage. In addition, Zhao et al. (2021) and Yuan et al. (2018) proposed that there exists a NE-trending, Jurassic, arc-related magmatic rock belt along the southeast coast of China. These suggest that the generation of the ca. 170–159 Ma PTS adakitic magmatic rocks was presumably related to an advancing subduction process during which compression gave rise to lithospheric thickening. Moreover, the identification of the ca. 176–158 Ma subducted slab (mainly the overlying sediments)-derived adakitic rocks in the interior of SE China, such as the Dexing volcanic-intrusive complex, Tongcun porphyry, and the Yuanzhuding granitoid porphyry (Fig. 1) suggests that subduction of the paleo-Pacific plate at least has reached eastern Jiangxi, and western Guangdong by ca. 160 Ma (Qiu et al., 2013; Zhong et al., 2013; Zhou et al., 2012). The formation of Late Jurassic A-type granite belt (ca. 165–150 Ma) following these ca. 176–158 Ma adakitic rocks in the interior of SE China (Fig. 1), further suggests that the extensional tectonic occurred only within a local area in the continental interior, and the coastal area of SE China during Jurassic remains a compressive tectonic setting with sparse magmatic activity, unequivocally corresponding to low-angle forward subduction of the paleo-Pacific plate (Fig. 11a). On the other hand, gradual episodic slab rollback of the paleo-Pacific plate migrated from inland to the coastal area during the Cretaceous was widely invoked to account for the generation of the Early Cretaceous A-type granite belt (ca. 140–125 Ma) and the Late Cretaceous A-type granite belt in SE China (ca. 101–86 Ma, Fig. 1; Li et al., 2022; Peng et al., 2021; Zhao et al., 2016), revealing an extensional tectonic regime during Cretaceous in the coastal area of SE China (Fig. 11b). Therefore, we conclude that subduction of the paleo-Pacific plate beneath the coastal area of SE China evolved from slab advance to slab rollback at ca. 145 Ma, resulting in a transition from a compressional (200–145 Ma) to an overall extensional (145–86 Ma) tectonic regime in the coastal belt of SE China (Fig. 11a and b).

Geochemically, the Middle-Late Jurassic PTS dacites and coexisting quartz diorite porphyries have extremely evolved Nd—Hf isotopic compositions with Neoarchean to Paleoproterozoic Nd—Hf model ages (ca. 2.75–1.94 Ga, Zhao et al., 2021 and this study), similar to those of the contemporary sporadical granitoids and their extrusive counterparts in the coastal area of SE China and the East China Sea Shelf (Figs. 7a and 8, Yuan et al., 2018; Zhao et al., 2021), suggesting their derivation from remelting of ancient basement rocks without significant involvement of mantle materials and ancient basement rocks similar to the Badu complex did are present in the eastern Cathaysia block (Zhao et al., 2021).

Noticeably, based on a compilation of this work and previous studies, zircon $\varepsilon_{Hf}(t)$ and whole-rock $\varepsilon_{Nd}(t)$ values for the magmatic rocks in the coastal area of SE China show a more depleted trend from the Middle Jurassic to the Late Cretaceous (Figs. 7 and 8), indicating that the contribution from a depleted asthenospheric mantle in their generation was gradually increasing. It is widely accepted that the gradual increase in the dip angle of the retreating paleo-Pacific plate during the Cretaceous, caused an increase in tectonic extension in the coastal area of SE China, as endorsed by the presence of numerous ca. 101–86 Ma extension-related rocks in coastal Fujian and Zhejiang Provinces (Zhao et al., 2015, 2016). This process induced more intensive underplating of mantle-derived magmas and increasing intensity of crust-mantle interaction in the coastal area of SE China. The underplating of mantle-derived magmas modified the components of continental crust and gave rise to the significant lithospheric rejuvenation during the Cretaceous in the coastal area of SE China, also as revealed by geophysical and petrological observations (Dong et al., 2020; Xu et al., 1996).

The continental crust in the coastal Cathaysia block was therefore mainly reworked during the Jurassic, but significantly modified and replaced by underplated mantle-derived depleted magma during the Cretaceous, which gave rise to continental crust growth and lays a foundation for the Cretaceous volcanic rocks having depleted Nd—Hf isotopic compositions.

5.4. A model of the magmatic system for the Late Cretaceous PTS volcanic-plutonic complex

Based on the above observations, we envision the following magmatic scenarios, and our model for the storage and evolution of the Late Cretaceous PTS magma system is schematically illustrated in Fig. 11. In the coastal Cathaysia Plate, the roll-back and steepening of the paleo-Pacific slab occurred during the Cretaceous and resulted in lithospheric extension and the underplating of mantle-derived basaltic melts (Fig. 11b). This process transitioned the lower continental crust from ancient basement rocks to newly-formed, mafic juvenile crust. The induced large-scale partial melting of the juvenile lower crust by mafic magma underplating gave rise to the formation of a deep massive acid magma reservoir in the mid-to-upper crust, leaving granulite residue in the lower crust (Zhao et al., 2016). Continued fractional crystallization and crystal accumulation in the shallow magma chamber formed the crystal mushes and the evolved, interstitial silicic melts (Bachmann et al., 2007). Evolved melt expulsion by compaction and repacking of the crystals in the mush generated the PTS minor-phase miarolitic granite, which simultaneously left the complementary crystal residue solidified as the main-phase granite (Fig. 11c, Bachman and Bachman, 2004; Bachmann and Huber, 2019; Solano et al., 2014). Subsequently, rejuvenation of the near-solidified crystal mush induced by hot mafic magma replenishment in the shallow magma reservoir led to the generation of the PTS strongly peraluminous rhyodacite and rhyolite (Fig. 11d). The recharge events of mafic magmas mainly are trapped at the base of the magma reservoir and do not propagate much higher because the silicic cumulate residues could act as mechanical barriers to the rising of recharge magmas (Du et al., 2022; Wark et al., 2007). This is evidenced by the fact that abundant microgranular mafic enclaves occur in the main-phase granite, but are scarce in the minor-phase miarolitic granite and erupted volcanic rocks. Meanwhile, crystallization and decompression drove fluid exsolution, and then possible fluid-melt interaction formed some of the terminal PTS rhyolites with significant REE tetrad effect, and potential Mo—Be mineralization (Rao et al., 2022).

Collectively, a complex long-lived, trans-crustal magmatic system in a back-arc extensional regime, which is dominated by crystal mush and periodically reactivated by new input of hot, mafic magma, is responsible for the generation of the PTS Cretaceous volcanic-plutonic complex as well as the contemporary ones in coastal Fujian and Zhejiang Provinces. It should be noted that the limited distribution and crustal origin of the Middle-Late Jurassic PTS dacite and quartz diorite porphyry imply a quick magma solidification after erupting and a relatively simple magma chamber process due to a less intense thermal regime in a compressive tectonic setting. Their rounded and embayed quartz and feldspar crystals without overgrowth of felsic minerals were products of rapid decompression during the eruption (Curry et al., 2021; Yan et al., 2022).

6. Conclusions

We report the newly discovered dacite, rhyodacite, rhyolite and subvolcanic miarolitic alkali-feldspar granite within the PTS volcanic-plutonic complex, which is predominantly composed of I-type alkali-feldspar granite (ca. 96–98 Ma), peralkaline A-type granites (ca. 86–88 Ma) and subordinate quartz diorite porphyry (ca. 170 Ma).

(1) New zircon U—Pb dating revealed that the dacites were produced at ca. 160 Ma, while the volcanic rocks and subvolcanic intrusions were crystallized practically identically within analytical errors at ca. 94–98 Ma.
(2) New results and compiled data indicate that the Paleoproterozoic crustal basement did widely occur in the eastern Cathaysia block, and were mainly reworked before the Cretaceous but significantly modified and replaced by the newly underplated mantle-derived depleted magma predominantly during the Cretaceous.
(3) The Jurassic and Late Cretaceous magmatic rocks within the PTS complex were generated in an advancing subduction compressive regime and a retreating subduction extensional regime of the paleo-Pacific plate, respectively. The Late Cretaceous PTS

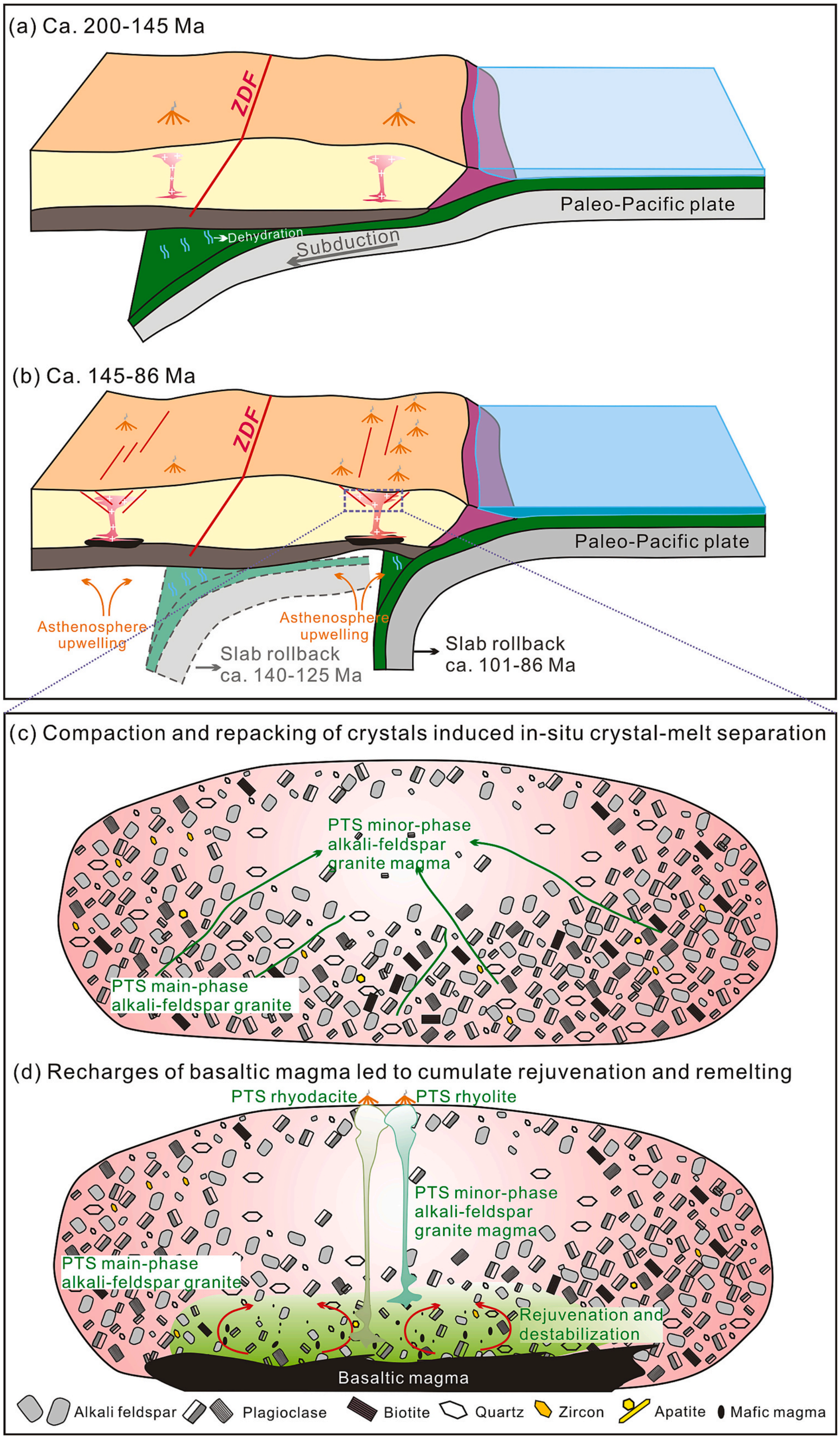

Fig. 11. Schematic cartoon for the tectonic processes (a and b) in the coastal regions of SE China during the late Mesozoic and the genesis of the Late Cretaceous PTS high-silica volcanic and plutonic rocks (c and d). Abbreviations: ZDF, Zhenghe–Dapu Fault.

volcanic-plutonic association is resulted from the long-lived transcrustal magmatic system, and the observed compositional diversity is probably attributed to crystal–melt segregation and rejuvenation of crystal mush facilitated by periodic recharge of hot mafic magmas as well as varying degrees of magma mixing in the shallow magma chamber.

Declaration of Competing Interest

The authors declared that we have no conflicts of interest to this work. We declare that we do not have any commercial or associative interest that represents a conflict of interest in connection with the work submitted.

Acknowledgments

We appreciate Prof. Jian-Sheng Qiu for his help with the manuscript. We thank Prof. Di-Cheng Zhu for handling this manuscript and two anonymous reviewers for constructive comments. We are grateful to Drs. Wan-Feng Chen, Cong-Hui Xiong, and Xiao-Li Yan at Lanzhou University, for their assistance during the experiment. This work was substantially supported by the National Natural Science Foundation of China (Grant Nos. 41702048, 42272096). Additional support was provided by the Youth Innovation Promotion Association, Chinese Academy of Sciences (No. 2020393).

Appendix A. Supplementary data

Supplementary data to this article can be found online at https://doi.org/10.1016/j.lithos.2023.107205.

References

Bachmann, O., Bergantz, G.W., 2004. On the origin of crystal-poor rhyolites: extracted from batholithic crystal mushes. J. Petrol. 45, 1565–1582.
Bachmann, O., Huber, C., 2019. The inner workings of crustal distillation columns; the physical mechanisms and rates controlling phase separation in silicic magma reservoirs. J. Petrol. 60 (1), 3–18.
Bachmann, O., Miller, C.F., Silva, S.L., 2007. The volcanic–plutonic connection as a stage for understanding crustal magmatism. J. Volcanol. Geotherm. Res. 167, 1–23.
Barnes, C.G., Werts, K., Memeti, V., Ardill, K., 2019. Most granitoid rocks are cumulates: deductions from hornblende compositions and zircon saturation. J. Petrol. 60, 2227–2240.
Bau, M., 1996. Controls on the fractionation of isovalent trace elements in magmatic and aqueous systems: evidence from Y/Ho, Zr/Hf, and lanthanide tetrad effect. Contrib. Mineral. Petrol. 123, 323–333.
Boynton, W.V., 1984. Geochemistry of the rare earth elements: Meteorite studies. In: Henderson, P. (Ed.), Rare Earth Elements Geochemistry. Elservier, Amsterdam, pp. 63–144.
Chen, J.F., Jahn, B., 1998. Crustal evolution of southeastern China: Nd and Sr isotopic evidence. Tectonophysics 284, 101–133.
Chen, Y.X., Li, H., Sun, W.D., Ireland, T., Tian, X.F., Hu, Y.B., Yang, W.B., Chen, C., Xu, D. R., 2016. Generation of late Mesozoic Qianlishan A_2-type granite in Nanling Range, South China: Implications for Shizhuyuan W-Sn mineralization. Lithos 266–267, 435–452.
Chen, J.Y., Yang, J.H., Zhang, J.H., 2019. Origin of cretaceous aluminous and peralkaline A-type granitoids in northeastern Fujian, coastal region of southeastern China. Lithos 340, 223–238.
Chen, J.Y., Yang, J.H., Zhang, J.H., Zhu, Y.S., 2021. Construction of a highly silicic upper crust in southeastern China: Insights from the cretaceous intermediate-tofelsic rocks in eastern Zhejiang. Lithos 402–403, 106012.
Corfu, F., Hanchar, J.M., Hoskin, P.W., Kinny, P., 2003. Atlas of zircon textures. Rev. Mineral. Geochem. 53, 469–500.
Curry, A., Caricchi, L., Lipman, P.W., 2021. Magmatic evolution of zoned and unzoned ignimbrites: evidence for a complex crustal architecture feeding four rapid-sequence, caldera-forming eruptions in the San Juan Mountains, Colorado. J. Petrol. 62, egab006.
Deering, C.D., Bachmann, O., Vogel, T.A., 2011. The Ammonia tanks Tuff: erupting a meltrich rhyolite cap and its remobilized crystal cumulate. Earth Planet. Sci. Lett. 310, 518–525.
Deering, C.D., Keller, B., Schoene, B., Bachmann, O., Beane, R., Ovtcharova, M., 2016. Zircon record of the plutonic-volcanic connection and protracted rhyolite melt evolution. Geology 44, 267–270.
Defant, M.J., Drummond, M.S., 1990. Derivation of some modern arc magmas by melting of young subducted lithosphere. Nature 347, 662–665.
Dong, C.W., Yang, S.F., Tang, L.M., Du, Z.Y., 2008. Petrology and Geochemistry of the Xinchang Composite Igneous Complexes, Zhejiang and their Geological Implication. Geol. J. China Univ. 14 (3), 365–376.
Dong, C.W., Yan, Q., Zhang, D.R., Du, Z.Y., Zhu, G.Q., 2010. Late Mesozoic extension in the coastal area of Zhejiang and Fujian provinces: a petrologic indicator from the Dongji Island mafic dike. Acta Petrol. Sin. 26 (4), 1195–1203.
Dong, S.W., Li, J.H., Cawood, P.A., Gao, R., Zhang, Y.Q., Xin, Y.J., 2020. Mantle influx compensates crustal thinning beneath the Cathaysia Block, South China: evidence from SINOPROBE reflection profiling. Earth Planet. Sci. Lett. 544, 116360.
Du, D.H., Wang, X.L., Wang, S., Miller, C.F., Xu, X., Chen, X., Zhang, F.F., 2022. Deciphering cryptic multi-stage crystal-melt separation during construction of the Tonglu Volcanic–Plutonic Complex, SE China. J. Petrol. 63 (1), 1–27.
Foley, S., Tiepolo, M., Vannucci, R., 2002. Growth of early continental crust controlled by melting of amphibolite in subduction zones. Nature 417 (6891), 837–840.
Frost, C.D., Frost, B.R., 2011. On ferroan (A-type) granitoids: their compositional variability and modes of origin. J. Petrol. 52 (1), 39–53.
Gan, C.S., Wang, Y.J., Zhang, Y.Z., Wang, Y., Qian, B., Sheldrick, T.C., Liu, Z., 2022. Early Jurassic high $\varepsilon_{Nd}(t)$-$\varepsilon_{Hf}(t)$ granites in the Southeastern South China Block: early Jurassic crustal growth or crustal reworking? J. Asian Earth Sci. 223, 104995.
He, Z.Y., Xu, X.S., 2012. Petrogenesis of the late Yanshanian mantle-derived intrusions in southeastern China: response to the geodynamics of paleo-Pacific plate subduction. Chem. Geol. 328, 208–221.
He, Z.Y., Xu, X.S., Niu, Y.L., 2010. Petrogenesis and tectonic significance of a Mesozoic granite-syenite-gabbro association from inland South China. Lithos 119 (3–4), 621–641.
Holness, M.B., 2018. Melt segregation from silicic crystal mushes: a critical appraisal of possible mechanisms and their microstructural record. Contrib. Mineral. Petrol. 173, 48.
Irber, W., 1999. The lanthanide tetrad effect and its correlation with K/Rb, Eu/Eu, Sr/Eu, Y/Ho, and Zr/Hf of evolving peraluminous granite suites. Geochim. Cosmochim. Acta 63, 489–508.
Jahn, B.M., Wu, F.Y., Capdevila, R., Martineau, F., Zhao, Z.H., Wang, Y.X., 2001. Highly evolved juvenile granites with tetrad REE patterns: the Woduhe and Baerzhe granites from the Great Xing'an Mountains in NE China. Lithos 59, 171–198.
Jiang, Y.H., Zhu, S.Q., 2017. Petrogenesis of the late Jurassic peraluminous biotite granites and muscovite-bearing granites in SE China: geochronological, elemental and Sr–Nd–O–Hf isotopic constraints. Contrib. Mineral. Petrol. 172 (11–12), 1–27.
Jiang, Y.H., Wang, G.C., Liu, Z., Ni, C.Y., Qing, L., Zhang, Q., 2015. Repeated slabadvance-retreat of the Palaeo-Pacific plate underneath SE China. Int. Geol. Rev. 57, 472–491.
Jiang, D.S., Erdmann, S., Deng, G.X., Guo, H.H., Wu, F., Xu, X.X., Xu, H., Zhao, Z.F., Huang, F., 2022. Barium isotope evidence for the generation of peralkaline granites from a fluid-metasomatized crustal source. Chem. Geol. 614, 121197.
Lee, C.T.A., Morton, D.M., 2015. High silica granites: Terminal porosity and crystal settling in shallow magma chambers. Earth Planet. Sci. Lett. 409, 23–31.
Li, Z.X., Li, X.H., 2007. Formation of the 1300-km-wide intracontinental orogen and postorogenic magmatic province in Mesozoic South China: a flat-slab subduction model. Geology 35 (2), 179–182.
Li, X.H., Chung, S.L., Zhou, H., Lo, C.H., Liu, Y., Chen, C.H., 2004. Jurassic intraplate magmatism in southern Hunan-eastern Guangxi: 40Ar/39Ar dating, geochemistry, Sr-Nd isotopes and implications for the tectonic evolution of SE China. Geol. Soc. Lond. Spec. Publ. 226 (1), 193–215.
Li, Z., Qiu, J.S., Yang, X.M., 2014. A review of the geochronology and geochemistry of late Yanshanian (cretaceous) plutons along the Fujian coastal area of southeastern China: Implications for magma evolution related to slab break-off and rollback in the cretaceous. Earth Sci. Rev. 128, 232–248.
Li, Y., Ma, C.Q., Xing, G.F., Zhou, H.W., Zhang, H., Brouwer, F.M., 2015. Origin of a cretaceous low-^{18}O granitoid complex in the active continental margin of SE China. Lithos 216–217, 136–147.
Li, X.Y., Li, S., Suo, Y., Huang, F., Wang, P., Luan, S., Zhou, J., 2022. High-silica rhyolites in the terminal stage of massive cretaceous volcanism, SE China: Modified crustal sources and low-pressure magma chamber. Gondwana Res. 102, 133–150.
Liu, L., Qiu, J.S., Li, Z., 2013. Origin of mafic microgranular enclaves (MMEs) and their host quartz monzonites from the Muchen pluton in Zhejiang Province, Southeast China: implications for magma mixing and crust–mantle interaction. Lithos 160–161, 145–163.
Liu, L., Hu, R.Z., Zhong, H., Tang, Y.W., Yang, J.H., Li, Z., Zhao, J.L., Shen, N.P., 2018. New constraints on the Cretaceous geodynamics of paleo-Pacific plate subduction: Insights from the Xiaojiang–Beizhang granitoids, Zhejiang Province, southeast China. Lithos 314–315, 382–399.
Liu, J.X., Wang, S., Wang, X.L., Du, D.H., Xing, G.F., Fu, J.M., Chen, X., Sun, Z.M., 2020. Refining the spatio-temporal distributions of Mesozoic granitoids and volcanic rocks in SE China. J. Asian Earth Sci. 201, 104503.
Liu, L., Yang, J.H., Kang, L.F., Zhong, H., Zhang, X.C., 2022. The long-lived transcrustal magmatic systems of Southeast China in response to paleo-Pacific plate subduction, recorded by the cretaceous volcanic sequences in southeastern Zhejiang Province. Geol. Soc. Am. Bull. https://doi.org/10.1130/B36448.1.
Lundstrom, C.C., Glazner, A.F., 2016. Silicic magmatism and the volcanic–plutonic connection. Elements 12, 91–96.
Macpherson, C.G., Dreher, S.T., Thirlwall, M.F., 2006. Adakites without slab melting: high pressure differentiation of island arc magma, Mindanao, the Philippines. Earth Planet. Sci. Lett. 243 (3–4), 581–593.
Maniar, P.D., Piccoli, P.M., 1989. Tectonic discrimination of granitoids. Geol. Soc. Am. Bull. 101, 635–643.
McDonough, W.F., Sun, S.S., 1995. The composition of the Earth. Chem. Geol. 120, 223–253.

Peccerillo, A., Taylor, D.R., 1976. Geochemistry of Eocene calc-alkaline volcanic rocks from the Kaitamonu area, Northern Turkey. Contrib. Mineral. Petrol. 58, 63–91.

Peng, H.W., Fan, H.R., Jiang, P., Hu, H.L., Lan, T.G., 2021. Two-stage rollbacks of the paleo-Pacific plate beneath the Cathaysia block during cretaceous: Insights from A-type granites and volcanic rocks. Gondwana Res. 97, 158–175.

Qiu, J.S., Wang, D.Z., Mclnnes, B.I.A., Jiang, S.Y., Wang, R.C., Kanisawa, S., 2004. Two subgroups of A-type granites in the coastal area of Zhejiang and Fujian Provinces, SE China: age and geochemical constraints on their petrogenesis. Trans. R. Soc. Edinb. Earth Sci. 95, 227–236.

Qiu, J.S., Li, Z., Liu, L., Zhao, J.L., 2012. Petrogenesis of the Zhangpu composite granite pluton in Fujian Province: constraints from zircon U–Pb ages, elements geochemistry and Nd–Hf isotopes. Acta Geol. Sin. 86 (4), 561–576 (in Chinese with English abstract).

Qiu, J.T., Yu, X.Q., Santosh, M., Zhang, D.H., Chen, S.Q., Li, P.J., 2013. Geochronology and magmatic oxygen fugacity of the Tongcun molybdenum deposit, Northwest Zhejiang, SE China. Mineral. Deposita 48, 545–556.

Rao, C., Wang, R., Wu, F., Che, X., Li, X., Wang, Q., Zhang, Z., Wu, R., 2022. A preliminary study on the volcanic intrusive complex type beryllium metallogenic belt from the southeast coast of China. Sci. China Earth Sci. 65 (8), 1586–1600.

Solano, J.M.S., Jackson, M.D., Sparks, R.S.J., Blundy, J.D., 2014. Evolution of major and trace element composition during melt migration through crystalline mush: implications for chemical differentiation in the crust. Am. J. Sci. 314, 895–939.

Vernon, R., Collins, W., 2011. Structural criteria for identifying granitic cumulates. J. Geol. 119 (2), 127–142.

Walker, B.A., Miller, C.F., Lowery Claiborne, L., Wooden, J.L., Miller, J.S., 2007. Geology and geochronology of the Spirit Mountain batholith, southern Nevada: Implications for timescales and physical processes of batholith construction. J. Volcanol. Geotherm. Res. 167 (1–4), 239–262.

Wark, D.A., Hildreth, W., Spear, F.S., Cherniak, D.J., Watson, E.B., 2007. Pre-eruption recharge of the Bishop magma system. Geology 35, 235–238.

Wong, J., Sun, M., Xing, G., Li, X., Zhao, G., Wong, K., Yuan, C., Xia, X., Li, L., Wu, F., 2009. Geochemical and zircon U-Pb and Hf isotopic study of the Baijuhuajian metaluminous A-type granite: extension at 125–100 Ma and its tectonic significance for South China. Lithos 112, 289–305.

Wu, F.Y., Liu, X.C., Liu, Z.C., Wang, R.C., Xie, L., Wang, J.M., Ji, W.Q., Yang, L., Liu, C., Khanal, G.P., He, S.X., 2020. Highly fractionated Himalayan leucogranites and associated rare-metal mineralization. Lithos 352 (353), 105319.

Wu, H., Zhang, Y., Wang, F.F., Song, W.Y., Bai, F.L., Xue, B.Y., Bi, S.P., 2022. Petrogenesis of cretaceous volcanic rocks from islands off Fujian Province, East China Sea, and implications for episodic slab rollback of the paleo-Pacific plate. Gondwana Res. 103, 243–259.

Xia, Y., Xu, X.S., Niu, Y.L., Liu, L., 2018. Neoproterozoic amalgamation between Yangtze and Cathaysia blocks: the magmatism in various tectonic settings and continent-arc-continent collision. Precambrian Res. 309, 56–87.

Xie, L., Wang, D.Z., Wang, R.C., Qiu, J.S., Chen, X.M., 2004. Complex zoning texture in plagioclase from the quartz diorite enclave in the Putuo granitc complex, Zhejiang Province: record of magma mixing. Acta Petrol. Sin. 20 (6), 1397–1408 (in Chinese with English abstract).

Xu, X.S., O'Reilly, S.Y., Zhou, X.M., Griffin, W.L., 1996. A xenolith-derived geotherm and the crust-mantle boundary at Qilin, southeastern China. Lithos 38, 41–62.

Xu, X.S., O'Reilly, S.Y., Griffin, W.L., Pearson, N.J., He, Z.Y., 2007. The crust of Cathaysia: age, assembly and reworking of two terranes. Precambrian Res. 158, 51–78.

Xu, X.S., Zhao, K., He, Z.Y., Liu, L., Hong, W.T., 2021. Cretaceous volcanic-plutonic magmatism in SE China and a genetic model. Lithos 402–403, 105728.

Xu, H., Qiu, J.S., Wang, X.L., Hong, Y.F., Wang, R.Q., Li, Y.F., 2022. Slow crystal settling controls the diversity of high-silica granites of the late cretaceous Shengsi Pluton at northeastern tip of Southeast China. J. Asian Earth Sci. 223, 104986.

Yan, L.L., He, Z.Y., 2022. Rejuvenation of silicic magmatic systems: Insights from the formation of garnet-bearing, crystal-rich tuff in Southeast China. Lithos 432–433, 106895.

Yan, L.L., He, Z.Y., Jahn, B.M., Zhao, Z.D., 2016. Formation of the Yandangshan volcanic–plutonic complex (SE China) by melt extraction and crystal accumulation. Lithos 266–267, 287–308.

Yan, L., He, Z., Beier, C., Klemd, R., 2018. Geochemical constraints on the link between volcanism and plutonism at the Yunshan caldera complex, SE China. Contrib. Mineral. Petrol. 173 (1), 4.

Yang, J.B., Zhao, Z.D., Hou, Q.Y., Niu, Y.L., Mo, X.X., Sheng, D., Wang, L.L., 2018. Petrogenesis of cretaceous (133–84 Ma) intermediate dykes and host granites in southeastern China: Implications for lithospheric extension, continental crustal growth, and geodynamics of Palaeo-Pacific subduction. Lithos 296–299, 195–211.

Yao, J.L., Shu, L.S., Cawood, P.A., Zhao, G.C., 2019. The Jiangnan Belt in South China: a ~970-820 Ma Rodinia margin accretionary orogen. Earth-Sci. Rev. 196, 102872.

Yin, S., Ma, C.Q., Xu, J.N., 2021. Recycling of K-feldspar antecrysts in the Baishiya porphyritic granodiorite, East Kunlun orogenic belt, northern Tibet Plateau: Implications for magma differentiation in a crystal mush reservoir. Lithos 402–403, 105622.

Yuan, W., Yang, Z.Y., Zhao, X.X., Santosh, M., Zhou, X.J., 2018. Early Jurassic granitoids from deep drill holes in the East China Sea Basin: implications for the initiation of Palaeo-Pacific tectono-magmatic cycle. Int. Geol. Rev. 60 (7), 813–824.

Zhang, X.L., Qiu, J.S., Wang, D.Z., Wang, R.C., Xu, X.S., Chen, X.M., 2005. Geochemistry and magmatic mixing of the Putuoshan biotite moyites and their enclaves, Zhejiang Province. Acta Petrol. Mineral. 24 (2), 81–92 (in Chinese with English abstract).

Zhao, J.L., Qiu, J.S., Liu, L., Wang, R.Q., 2015. Geochronological, geochemical and Nd–Hf isotopic constraints on the petrogenesis of late cretaceous A-type granites from the southeastern coast of Fujian Province, South China. J. Asian Earth Sci. 105, 338–359.

Zhao, J.L., Qiu, J.S., Liu, L., Wang, R.Q., 2016. The late cretaceous I- and A-type granite association of Southeast China: Implications for the origin and evolution of postcollisional extensional magmatism. Lithos 240–243, 16–33.

Zhao, J.L., Qiu, J.S., Liu, L., 2021. Early-Middle Jurassic arc-related magmatic rock belt along SE China coast: Petrogenesis and implications for paleo-Pacific plate subduction. J. Asian Earth Sci. 210, 104687.

Zhong, L.F., Li, J., Peng, T.P., Xia, B., Liu, L.W., 2013. Zircon U–Pb geochronology and Sr–Nd–Hf isotopic compositions of the Yuanzhuding granitoid porphyry within the Shi-Hang Zone, South China: Petrogenesis and implications for Cu–Mo mineralization. Lithos 177, 402–415.

Zhou, X.M., Sun, T., Shen, W.Z., Shu, L.S., Niu, Y.L., 2006. Petrogenesis of Mesozoic granitoids and volcanic rocks in South China: a response to tectonic evolution. Episodes 29, 26–33.

Zhou, Q., Jiang, Y.H., Zhao, P., Liao, S.Y., Jin, G.D., 2012. Origin of the Dexing Cubearing porphyries, SE China: elemental and Sr–Nd–Pb–Hf isotopic constraints. Int. Geol. Rev. 54 (5), 572–592.

Zhou, Y., Liang, X.Q., Wu, S.C., Cai, Y.F., Liang, X.R., Shao, T.B., Wang, C., Fu, J.G., Jiang, Y., 2015. Isotopic geochemistry, zircon U–Pb ages and Hf isotopes of A-type granites from the Xitian W–Sn deposit, SE China: Constraints on petrogenesis and tectonic significance. J. Asian Earth Sci. 105, 122–139.